RSC Advances

Synthesis and assessment of photoluminescence properties of Ca4-2xAl6WO16:REx,Nax (RE = Eu3+, Dy3+ and Sm3+) phosphors

Journal:	*RSC Advances*
Manuscript ID:	RA-ART-05-2015-009291.R1
Article Type:	Paper
Date Submitted by the Author:	14-Jun-2015
Complete List of Authors:	DABRE, KAMLESH; Taywade College, Koradi, Physics Dhoble, Sanjay; RTM Nagpur University, Nagpur, Physics

Synthesis and assessment of photoluminescence properties of $Ca_{4-2x}Al_6WO_{16}:RE_x,Na_x$ (RE = Eu^{3+}, Dy^{3+} and Sm^{3+}) phosphors

K.V. Dabre[a] and S.J. Dhoble[b*]

[1]Deptartment of Physics, Taywade College, Koradi, Nagpur-441111, India

[2]Department of Physics, R.T.M. Nagpur University, Nagpur-440033, India

*Corresponding author email: kamleshdbr@yahoo.com Tel: +91 8446823689

Abstract

In present work, rare earth (Eu^{3+}, Dy^{3+} and Sm^{3+}) activated $Ca_4Al_6WO_{16}$ phosphors were synthesized by citrate complexation and combustion methods and their photoluminescence characterization was performed. Phase purity and morphology of the phosphor were characterized by XRD and SEM. The SEM micrographs of phosphor sample synthesized by citrate complexation method show layer structure while sample synthesized by citrate combustion method show porous nature. Intense red emission of Eu^{3+} and yellow emission of Dy^{3+} in $Ca_4Al_6WO_{16}$ host lattice show the occupation of noncentrosymmetric site by the rare earth ions in host lattice. The reddish orange emission from Sm^{3+} activated phosphor consists of three intense emission peaks in yellow, orange-red and red region respectively at 567, 604 and 650nm. Intense characteristic emissions show no concentration quenching up to 2mol% concentration of rare earth ions. The phosphors could be effectively excited by near UV (Dy^{3+} activated phosphor) and visible light (Eu^{3+} and Sm^{3+} activated phosphors) and give emission hues from orange-red to near white which claim their potential candidature for the application in solid state lighting.

Keywords: $Ca_4Al_6WO_{16}$; Citrate complexation; Citrate Combustion; Photoluminescence;

1. Introduction

Now days, light emitting diodes (LEDs) as solid state lighting (SSL) devices plays an important role in reducing the growing problems of environment and energy crises. The requirement of efficient optical materials forces researchers to explore novel optical materials especially rare earth doped phosphors[1-4]. The unique electronic and optical properties of rare earth ions attract researchers attention for the development of such phosphor which could fulfill the requirements of the growing technology's demand[5,6]. In this respect many of the rare earth activated host materials have been continuously

investigated, but we are fascinated by the tungstate based phosphors because of their self-activation, good stability for physical conditions (chemical and thermal) and wider applicability in various fields such as scintillation, solid state laser, electro-optic applications, catalytic etc. It is very well known that tungstates materials without inversion symmetry (noncentrosymmetric) are largely studied as competitive host materials in the optical field due to their promising applications for laser, optical fibers and scintillators as phosphors. Especially tungstates with rare earth (lanthanide) ions activation are well studied[7-16]. In fact, noncentrosymmetric compounds are of particular interest because their symmetry-dependent properties such as piezoelectricity, ferroelectricity, and second-order nonlinear optical behavior are the basis of numerous applications[17].

The optical properties of alumino-tungstate phosphors are rarely are sparsely investigated. However, Liu et al.[18] have shown interesting luminescence properties of $Ca_8[Al_{12}O_{24}](WO_4)_2:Tb^{3+}$ phosphor synthesized by solid state reaction method. Hong et al.[19] has reported interesting luminescence properties of novel Eu^{3+} activated alumino-tungstate ($Ca_4Al_6WO_{16}$) phosphors synthesized by combustion method, and found to be potential candidate for near-UV LEDs. Varieties of methods are available for the synthesis of the tungstate based phosphors, but in this work, we utilized citrate complexation and combustion methods for the synthesis of rare earth (Eu^{3+}, Dy^{3+} and Sm^{3+}) activated $Ca_4Al_6WO_{16}$ phosphors and their photoluminescence (PL) properties were studied.

2. Material and Methods

Calcium nitrate [$Ca(NO_3)_2 .4H_2O$], aluminum nitrate [$Al(NO_3)_2 .9H_2O$], tungstic acid (H_2WO_4), sodium tungstate (Na_2WO_4), citric acid ($C_6H_8O_7 .H_2O$), ethylene glycol ($C_2H_6O_2$), 25% ammonia (NH_3) solution and 69-71% nitric acid (HNO_3) were analytically pure (99.9%) and used without further purification for the synthesis of $Ca_4Al_6WO_{16}$. For the rare earth (Eu^{3+}, Dy^{3+} and Sm^{3+}) doping the analytically pure (99.99%) rare earth oxides [RE_2O_3 (RE = Eu, Dy and Sm)] were used. The details of methods of synthesis employed in this work viz. citrate complexation and citrate combustion methods are given as follows.

Fig. 1. The schematics of citrate complexation and citrate combustion synthesis methods for the synthesis of $Ca_{4-2x}Al_6WO_{16}:RE_x,Na_x$ (RE = Eu^{3+}, Dy^{3+} and Sm^{3+}) phosphors.

Fig. 1 illustrates the schematics of citrate complexation and citrate combustion synthesis methods employed in this work for the synthesis of $Ca_{4-2x}Al_6WO_{16}:RE_x,Na_x$ (RE =

Eu^{3+}, Dy^{3+} and Sm^{3+}) phosphors. In typical synthesis, H_2WO_4 was added in the solution of H_2O (distilled) and NH_3 (1:1) and continuously stirred at 80°C for at least 1 Hr until the solution became clear. Simultaneously the solutions of $C_6H_8O_7.H_2O$, $Al(NO_3)_3$ and $Ca(NO_3)_2$ in distilled H_2O was made separately. The solution of $C_6H_8O_7.H_2O$ was added to the clear solution of H_2WO_4 drop wise at room temperature with continuous stirring for 1 Hr, the solution remains clear and it termed as solution A. The pH of the solution A was maintained within 2 and 3 by adding NH_3 solution. Hydrated citric acid was the source of citrate anion that was used as both chelating agent to metal cations and fuel for the combustion. To guarantee an excess of chelating agent are added in the ratio 1:1 to metal cations. Then the solutions of $Al(NO_3)_3$ and $Ca(NO_3)_2$ were added drop wise sequentially in solution A with continuous stirring in the interval of 1 Hr; the final solution of citrate complex with metal cations was termed as solution C which still remains clear. This route to obtain solution C was common for both citrate complexation and citrate combustion method. For the synthesis of rare earth doped samples rare earth oxide was dissolved in concentrated HNO_3 and excess of HNO_3 is evaporated. This rare earth nitrate solution was added in solution A before adding solutions of $Al(NO_3)_3$.

In citrate complexation method, the solution C was continuously stirred for 1 Hr. Thereafter, $C_2H_6O_2$ was added drop vise to promote the esterification reaction, which polymerizes the individual metal citrate complex. The molar ratio between $C_6H_8O_7.H_2O$ and $C_2H_6O_2$ was kept at 3:2. The solution became turbid with yellowish brown color. Then this solution mixture was covered and continuously stirred at 80°C for 12 Hrs. to drive off all the solvent. The gel initially started to swell and filled the beaker producing a foamy brown color gel. This foam consists of very light and homogeneous flakes of small particles. This solid brown gel was softly milled to powder and calcined at 350°C for 12 Hrs. to remove organic contents and a black precursor was formed. This black precursor was further calcined at 800°C for 12 Hrs. and results in white body phosphor which was finally calcined at 1200°C for 4 Hrs. and allowed to cool to room temperature inside the furnace by switching it off. In citrate combustion method, the solution C was continuously stirred with heating at 80°C for 4 Hrs. to obtain highly viscous gel solution. This gel solution was transferred to the porcelain crucible and kept in preheated vertical furnace at 500°C. An auto-combustion process took place accompanied by the evolution of brown fumes and after completion of combustion process dark brown solid foam was remained. Thereafter, this brown solid foam was crushed to powder and calcined at 800°C for 12 Hrs. to obtain white

body phosphor. Finally, this white phosphor was fired at 1200^{o}C for 4 Hrs. and allowed to cool slowly in the furnace by switching it off.

The phase purity and structural analysis of the sample was examined by X-ray diffraction (XRD) pattern which was obtained at room temperature from PANalytical X'Pert Pro X-ray diffractometer with Cu Kα radiation (λ = 1.5406A^{0}). The morphology of the sample surface was analyzed by micrograph of the sample which is recorded on scanning electron microscope (SEM) (JEOL/EO, JSM-6380). The room temperature PL excitation and emission spectra of as synthesized samples were recorded on the Shimadzu RFPC5301 Spectrofluorophotometer with constant spectral slit width of 1.5nm.

3. Result and Discussion

The crystallinity and phase purity of undoped samples of $Ca_4Al_6WO_{16}$ synthesized by both citrate complexation and citrate combustion method were examined by XRD pattern and is shown in **Fig. 2**. The XRD patterns of both samples are very similar in nature and show good agreement with standard JCPDS PDF (#75-0697). The as-synthesized samples exhibits orthorhombic phase [space group Aba2 (No. 41)] with lattice parameter values are a = 26.15A^{o}, b = 13.07A^{o} and c = 9.319A^{o} and α = β = γ = 90^{o}. However, Hong et al.[19] reports the formation of tetragonal phase with space group P-4c2 (No. 116) which is in contradiction to the present observation. $Ca_4Al_6WO_{16}$ has both tetragonal and orthorhombic phases which could be derived from parent cubic phase. Thus, it could be assumed that there is existence of both tetragonal and orthorhombic phases[20].

Fig. 2. XRD patterns of $Ca_4Al_6WO_{16}$ synthesized by (a) citrate complexation, (b) citrate combustion methods and (c) standard JCPDS PDF #75-0697.

The average crystallite size (D) was determined using Debye-Scherrer formula as given below[21],

$$D = \frac{0.9\lambda}{\beta \cos\theta}$$

Where λ is the wavelength of the X-ray radiation, β is the full-width at half-maximum (FWHM) and θ is the angle of diffraction peak. The average crystallite size of the samples synthesized by complexation and combustion methods was found to be 370 and 430nm

respectively, which shows the formation of sub-micron phosphor. Thus, one can obtain nanocrystalline phosphor sample by opting citrate complexation method.

Fig. 3. SEM micrographs of $Ca_4Al_6WO_{16}$ synthesized by (a) citrate complexation and (b) citrate combustion methods.

It is well known that the luminescence properties of phosphor materials depend on the morphology of the particles, such as shape, size, size distribution, defects, and so on. The microstructure and morphology of the samples were investigated by SEM micrographs. **Fig. 3** depicts the SEM micrographs of $Ca_4Al_6WO_{16}$ samples. The typical SEM micrographs of the samples synthesized by citrate complexation and combustion methods show the layer structure and porous structure respectively with pronounced agglomeration. It is well understood that the same material could exhibit different morphologies if it is synthesized by different routes. In combustion synthesis the rapid evolution of the gases takes place which result in the formation of the porous nature of the phosphor sample while, in the complexation process the molecules gets enough time to orient in proper direction due to prolong stirring under controlled environment, thus forming layer structure. During the progress of reaction the atoms orientated in particular fashion to form typical microstructure which is highly dependent on pH of the reaction mixture. The micrographs of the both samples show pronounced agglomeration due to the post synthesis heat treatment at high temperature (1200^oC) which facilitates the nucleation and growth of the grains due to increase in atomic mobility. The average grain size could be in sub-micron range which confirms the calculation from XRD pattern, but it is difficult to measure the actual grain size distribution due to agglomeration and low magnification of present SEM micrographs.

Fig. 4. PL excitation spectra of $Ca_{4-2x}Al_6WO_{16}:Eu_x,Na_x$ (2mol%) phosphor with emission monitored at (a) 442nm and (b) 617nm.

The room temperature excitation spectra of $Ca_4Al_6WO_{16}$ (**Fig.4a**) and $Ca_{4-2x}Al_6WO_{16}:Eu_x,Na_x$ (2mol%) phosphor by monitoring the intrinsic tungstate group emission at 442 (**Fig.4a**) and characteristic emission of Eu^{3+} at 617nm (**Fig.4b**) respectively. It is observed that the excitation spectra of blue emission (442nm) consists of broad band in the vicinity of 220-280nm having maximum at around 240nm which correspond to the transition of charge transfer (CT) type from filled 2p orbitals of O^{2-} to empty 5d orbitals of W^{6+} within $(WO_4)^{2-}$ complex. The excitation spectra of red emission (617nm) consists of a broad band in the vicinity of 250-350nm having maximum at 286nm and number of sharp

peaks centered at 362, 377, 384, 395, 410, and 466nm. The broad band attributes to interweaved CT band of W^{6+}-O^{2-} and Eu^{3+}-O^{2-}. The sharp peaks in near UV and visible region are characteristics of intra f-f transition of Eu^{3+} and are attributed to the transitions from ground state $^7F_0$ to respective excited states $^5D_4$ (362nm), $^5G_{4,5,6}$ (377nm), $^5L_7$, $^5G_{2,3}$ (384nm), $^5L_6$ (395nm), $^5D_3$ (410nm) and $^5D_2$ (466nm). One weak sharp peak is also observed at 417nm which is attributed to $^7F_1 \rightarrow {}^5D_3$ transition which indicates that the higher levels of Eu^{3+} is also populated with few of electrons at room temperature[22].

Fig. 5. PL emission spectra of $Ca_{4-2x}Al_6WO_{16}:Eu_x,Na_x$ (2mol%) phosphor excited at 240nm.

Fig. 5 shows the emission spectra of $Ca_{4-2x}Al_6WO_{16}:Eu_x,Na_x$ (2mol%) phosphor excited at 240nm. Under the excitation of 240nm the emission spectra show a broad band extending from violet to red region of visible spectrum and having peak in blue region (at around 442nm). This broad band is attributed to CT transition within $(WO_4)^{2-}$ complex and termed as annihilation of self-trapped exciton. In addition, one weak narrow peak is also observed at 614nm in red region which is characteristic of intra f-f transition of Eu^{3+} ion and the emission intensity is higher in the sample synthesized by complexation method than combustion method. This indicates the energy transfer from $(WO_4)^{2-}$ complex to Eu^{3+} ion, but the extent of energy transfer is very less.

Fig. 6. (a) PL emission spectra of $Ca_{4-2x}Al_6WO_{16}:Eu_x,Na_x$ (2mol%) phosphor excited at 466nm. (b) Variation of emission intensity with Eu^{3+} concentration in phosphor.

The distorted surrounding of Eu^{3+} and its reduced crystal symmetry could be useful to achieve better color purity and improvement in chromaticity of phosphor material. Under the blue excitation of 466nm ($^5D_2$) the emission spectra of $Ca_{4-2x}Al_6WO_{16}:Eu_x,Na_x$ (2mol%) phosphor (**Fig. 6a**) shows the number of sharp emission peaks in orange and red spectral region at 581, 589, 593, 614, 617nm. These emission peaks are characteristics of intra f-f transitions of Eu^{3+} ion and are attributed to $^5D_0 \rightarrow {}^7F_J$ (J = 0, 1 and 2) transitions. Out of all emission peaks the predominant emission in red region at 614 and 617nm are due to the $^5D_0 \rightarrow {}^7F_2$ transition of Eu^{3+}; this result in good chromaticity coordinates (x = 0.593, y = 0.405). In addition, in the emission spectra a strongly forbidden $^5D_0 \rightarrow {}^7F_0$ transition at 581nm is observed and also the intensity of peak due to magnetic dipole (MD) ($^5D_0 \rightarrow {}^7F_1$) transition at 589 and 593nm is very weak than hypersensitive electric dipole (ED) ($^5D_0 \rightarrow {}^7F_2$) transition of Eu^{3+} ion. This leads to the conclusion that Eu^{3+} ions is substituted at the site lacking inversion symmetry i.e noncentrosymmetric site in the host lattice[22,23]. The emission

intensity of red peak is found to be increases with Eu^{3+} concentration (**Fig. 6b**) and no concentration quenching was observed up to 2mol%.

Fig. 7. PL excitation spectra of $Ca_{4-2x}Al_6WO_{16}:Dy_x,Na_x$ (2mol%) phosphor by monitoring emission at 578nm.

Fig. 7 shows the room temperature PL excitation spectra of $Ca_{4-2x}Al_6WO_{16}:Dy_x,Na_x$ (2mol%) phosphor by monitoring yellow emission at 578nm. The excitation spectra of characteristic yellow emission (578nm) of $Ca_{4-2x}Al_6WO_{16}:Dy_x,Na_x$ (2mol%) phosphor synthesized by both method exhibit same nature and consists of a broad band in the vicinity of 220-330nm and peaking at 253nm and number of sharp characteristic peaks in near UV spectral region (350-400nm). Unlike to Eu^{3+} ion the CT band of Dy^{3+} ion is located below 200nm[24]; thus, the broad band in UV region having maximum at 253nm is solely attributed to the ligand to metal CT transition from oxygen to tungsten in $(WO_4)^{2-}$ tetrahedral complex. The excitation spectra of both phosphors also consists of intense sharp excitation peaks in near UV region at 325, 351, 366 and 385nm which are characteristic of intra f-f transitions of Dy^{3+} ion and are attributed to transition from ground state $^6H_{15/2}$ to respective excited states $^4K_{15/2}$, $^4M_{15/2}+^6P_{7/2}$, $^6P_{5/2}$ and $^4M_{21/2}+^4F_{17/2}+^4F_{7/2}+^4I_{13/2}$[25,26].

Fig. 8. PL emission spectra of $Ca_{4-2x}Al_6WO_{16}:Dy_x,Na_x$ (2mol%) phosphor excited at 385nm. In inset, the variation of intensity of blue (485nm) and yellow (578nm) peak with Dy^{3+} ion concentration in $Ca_4Al_6WO_{16}$ synthesized by complexation method.

It is well known that the color of the Dy^{3+} ion luminescence is close to white. **Fig. 8** shows the room temperature PL emission spectra of Dy^{3+} activated phosphor under near UV excitation of 385nm. The emission spectra of both phosphor is relatively same and consists of two sharp bands in blue (485nm) and yellow (578nm) spectral region which are attributed to the $^4F_{9/2} \rightarrow {}^4H_{15/2}$ and $^4F_{9/2} \rightarrow {}^4H_{13/2}$ transitions of Dy^{3+} ion respectively. The $^4F_{9/2} \rightarrow {}^4H_{13/2}$ transition belongs to hypersensitive ED transition, which is strongly influenced by local symmetry environment of Dy^{3+} ion in host lattice[27]. This confirms the conclusion derived from Eu^{3+} luminescence in $Ca_4Al_6WO_{16}$ that rare earth ion occupy the noncentrosymmetric site in the host lattice. The luminescence intensity of Eu^{3+} and Dy^{3+} activated $Ca_4Al_6WO_{16}$ phosphor synthesized by complexation method is found to be more than the one synthesized by combustion method. The luminescence performance of phosphor is related to the radiative recombination of electrons and holes at luminescence center. However, losses of excitation energy occur due to migration of electrons and holes

through material towards surface and recombine non-radiatively at quenching center. As already stated that the microstructure and morphology of phosphor depends on method of synthesis which could affects the luminescence performance of the phosphor. The combustion synthesis is accompanied by rapid evolution of gasses which results in greater extent of surface defects which acts as luminescence quenching centers. However, complexation process is lengthy which leads to formation of surface defects in lesser extent. Hence, the luminescence intensity of the phosphor synthesized by complexation method is higher than combustion method[28]. Thus, it is claimed that the citrate complexation method is suitable for the synthesis of $Ca_{4-2x}Al_6WO_{16}:RE_x,Na_x$ phosphor to obtain better luminescence properties. Thereafter, the Dy^{3+} and Sm^{3+} activated $Ca_4Al_6WO_{16}$ phosphor samples were synthesized only by citrate complexation method.

The influence of Dy^{3+} ion concentration in host lattice on luminescence properties of phosphor was also investigate and is shown in inset of **Fig. 8**. It is seen that the intensity of both blue and yellow peak increases linearly with Dy^{3+} concentration in $Ca_4Al_6WO_{16}$ up to 2mol% without quenching. The intensity ratio of yellow and blue peak is nearly constant up to 1mol% and it is increases for 2mol% which changes the color of the phosphor; thus, the color of the phosphor can be tuned for white emission by adjusting yellow to blue intensity ratio, i.e by changing Dy^{3+} ion concentration.

Fig. 9. (a) PL excitation (λ_{em} = 604nm) spectrum of $Ca_{4-2x}Al_6WO_{16}:Sm_x,Na_x$ (2mol%) phosphor. (b) Energy level scheme of $4f^5$ configuration of Sm^{3+} ion showing various transitions related to various excitation and emission peaks.

Trivalent samarium ion with $4f^5$ configuration is known for its complicated energy levels and various possible intra f-f transitions. The room temperature excitation and emission spectra of Sm^{3+} activated $Ca_4Al_6WO_{16}$ phosphor are shown in **Fig. 9** and **10**. The excitation spectrum is consists of a broad band in UV (220-320nm) region having maximum at 275nm and some sharp characteristic peaks in visible region (400-500nm). The broad band in UV region is mainly attributed to the CT band of Sm^{3+} - O^{2-} and W^{6+} - O^{2-}; the series of sharp peaks in visible region are characteristics of intra f-f transition of Sm^{3+} ion as shown in energy level scheme of Sm^{3+} ion in **Fig. 9b**.

Fig. 10. PL emission spectra of $Ca_{4-2x}Al_6WO_{16}:Sm_x,Na_x$ (2mol%) phosphor. In inset, the variation of intensity of yellow (567nm), orange-red (604nm) and red (650nm) peaks with Sm^{3+} concentration.

The reddish orange emission from Sm^{3+} activated $Ca_4Al_6WO_{16}$ phosphor (**Fig. 10**) consists of three narrow and intense emission peaks in visible region at 567, 604 and 650nm, which are assigned to the intra f-f transitions from the excited level $^4G_{5/2}$ to ground levels $^6H_{5/2}$, $^6H_{7/2}$ and $^6H_{9/2}$ respectively[29]. The position and intensity of characteristic peaks remains same for both CT band (275nm) and line (410nm) excitation; this shows that the Sm^{3+} ion substituted at only one site in host lattice. Sm^{3+} activated phosphor excited at 275nm also shows weak broad emission band related to $(WO_4)^{2-}$ complex in blue green region in addition to the intense characteristic emissions of Sm^{3+} ion; this indicate the efficient energy transfer from $(WO_4)^{2-}$ complex to Sm^{3+} ion. The intensity of all three characteristic emission peaks of Sm^{3+} ion are increases with Sm^{3+} ion concentration in host lattice (inset of **Fig. 10**) and no luminescence quenching is observed up to 2mol% concentration of Sm^{3+} ion.

Judd-Ofelt (JO) theory[30,31] plays very crucial role in analyzing spectral properties of rare earth ion in different host materials. To interpret the luminescence properties of RE^{3+} ion three JO intensity parameter $\Omega_{(k)}$ (k = 2, 4 and 6) were calculated from PL spectra which are related with transition line strength (S) as[32],

$$S = e^2 \sum_{k=2,4,6} \Omega_{(k)} \left| \left\langle 4f^N (S,L) J \left\| U^{(k)} \right\| 4f^N (S',L') J' \right\rangle \right|^2 \qquad (1)$$

Table 1. Intensity parameters $\Omega_{(k)}$ (k = 2,4,6) (in the unit of 10^{-20} cm^2) of $CaAl_6WO_{16}:RE^{3+}$ (RE = Eu, Dy and Sm) phosphors.

Where, $U^{(k)}$ is matrix element of spherical tensor operator and the reduce matrix element $\left\langle 4f^N (S,L) J \left\| U^{(k)} \right\| 4f^N (S',L') J' \right\rangle$ of Eu^{3+}, Dy^{3+} and Sm^{3+} ions were directly taken from the compilation by Carnall et al.[33]. The experimental oscillator strength (f_{exp}) of exciting line was calculated using expression:

$$f_{\exp} = \frac{8\pi^2 m_e c \chi}{3h\lambda e^2 (2J+1)} S \qquad (2)$$

Where, m_e is mass of electron, c is velocity of light, h is planks constant, λ is wavelength e is electronic charge and χ is local field correction factor and is equal to $n(n^2+2)^2/9$ where 'n' is refractive index of the material. Unfortunately, there is no data in the literature reporting refractive index of $CaAl_6WO_{16}$; however, owing to the similar structure of $CaAl_6WO_{16}$ and sodalite, it is sensible to use the refractive index of sodalite (1.48) for the calculation of luminescence parameters. The experimental JO intensity parameter $\Omega_{(k)}$ (k = 2, 4 and 6) for Eu^{3+}, Dy^{3+} and Sm^{3+} ions activated $CaAl_6WO_{16}$ phosphor are compiled in **table 1**. The intensity parameter $\Omega_{(2)}$ is related to the degree of covalency at RE^{3+} site in the host matrix and larger value of $\Omega_{(2)}$ indicates the highly covalence nature of RE^{3+}-ligand bond. The parameter $\Omega_{(4)}$ and $\Omega_{(6)}$ is associated with the rigidity of the host matrix and they are found to be decrease with increase in rigidity of the matrix and shows larger values for glasses, organic, hybrid material etc.[34,35]. The derived intensity parameter $\Omega_{(2)}$ is greater than $\Omega_{(4)}$ and $\Omega_{(6)}$ which indicates the covalent nature of RE^{3+}-O^{2-} bond. Once the JO intensity parameter are determined it is easy to calculate the spontaneous radiative transition probability various transitions in emission spectra can be computed by the expression[35,36]:

$$A_{J\to J'} = \frac{64\pi^2 e^2 \chi}{3h\lambda^3(2J+1)} S \qquad (3)$$

The radiative lifetime of various transitions can be calculated by summing up the radiative transition probabilities from one excited state J to all possible lower state J' by the equation:

$$\tau_{rad} = \frac{1}{\sum_{J'} A_{J\to J'}} \qquad (4)$$

and finally, the branching ratios which gives the fractional contribution of particular radiative transition in total radiative decay of that excited state and can be given as:

$$\beta_{J\to J'} = \frac{A_{J\to J'}}{\sum_{J'} A_{J\to J'}} \qquad (5)$$

Table 2. Luminescence parameters for Eu^{3+}, Dy^{3+} and Sm^{3+} ions activated $CaAl_6WO_{16}$ phosphor at room temperature.

Fig. 11. The CIE chromaticity coordinates of $Ca_{4-2x}Al_6WO_{16}:RE_x,Na_x$ [RE = (a) Eu, (b) Dy and (c) Sm] phosphors on 1931 CIE chromaticity diagram.

The luminescence parameters for Eu^{3+}, Dy^{3+} and Sm^{3+} ions activated $CaAl_6WO_{16}$ phosphor at room temperature are presented in **table 2**. The calculated radiative lifetime for Eu^{3+}, Dy^{3+} and Sm^{3+} ions activated $CaAl_6WO_{16}$ phosphor is found to be 1.46, 1.59 and 1.26ms respectively. To evaluate the performance of phosphor material on color luminescent emission, CIE chromaticity coordinates were calculated and are presented on 1931 CIE chromaticity diagram as shown in **Fig. 11**. The intense red and weak orange-red emission of Eu^{3+} in activated $Ca_4Al_6WO_{16}$ phosphor gives reddish orange (x = 0.593, y = 0.405) appearance to the phosphor. The presence of three intense yellow, orange-red and red peaks in emission spectra of Sm^{3+} in activated $Ca_4Al_6WO_{16}$ phosphor, the phosphor hue appears to be yellowish orange (x = 0.428, y = 0.387). By adjusting proper intensity ratio of characteristic yellow and blue peaks of Dy^{3+} ion, the near white emission from the phosphor could be achieved, but in present case the intensity of yellow peak in both Dy^{3+} activated $Ca_4Al_6WO_{16}$ phosphor synthesized by complexation and combustion method are 2.42 and 1.99 times higher than blue peak which gives the phosphor a pale yellowish appearance [(x = 0.382, y = 0.410) and (x = 0.372, y = 0.402)].

4. Conclusion

In summary, we have successfully synthesized rare earth (Eu^{3+}, Dy^{3+} and Sm^{3+}) activated $Ca_4Al_6WO_{16}$ submicron phosphors by citrate complexation and combustion methods. The XRD and SEM result reveals the formation of desired orthorhombic phase with average crystallite size of 370 and 470nm by complexation and combustion methods respectively. Variation in morphology of the phosphor samples is observed with the change in synthesis method. The rare earth ions are substituted at noncentrosymmetric site in $Ca_4Al_6WO_{16}$ host lattice. Efficient energy transfer is observed in between tungstate and Sm^{3+} ion than Eu^{3+} and Dy^{3+} ions. For all three rare earth ions the PL emission intensity did not quenched up to the 2mol% concentration in host lattice. The nature of emission and excitation spectra of the phosphors synthesized by both methods is identical. However, the intensity of the phosphor synthesized by citrate complexation method is higher than citrate combustion method. The citrate complexation method is found to be better than citrate combustion method for the synthesis of $Ca_{4-2x}Al_6WO_{16}:RE_x,Na_x$ (RE = Eu^{3+}, Dy^{3+} and Sm^{3+}) phosphors to obtain good crystallinity and optical properties. The emission hue of the phosphor could be tuned from orange-red to near white by selecting proper activator.

Reference:

1 Y. Liu, Y. Wang, L. Wang, Y.Y. Gu, S.H. Yu, Z.G. Lu, and R. Sun, *RSC Adv*., 2014, **4**, 4754.

2 A.M. Kaczmareka and R. Van Deun, *Chem. Soc. Rev.*, 2013, **42**, 8835.

3 N.G. Yeh, C.H. Wu and T.C. Cheng, *Renew Sustain Energy Rev,* 2010, **14**, 2161.

4 N. Yeh and J.P. Chung, *Renew Sustain Energy Rev,* 2009, **13**, 2175.

5 Y. Zhou and B. Yan, *CrystEngComm*, 2013, **15**, 5694.

6 K.V. Dabre and S.J. Dhoble, *J. Lumin*. 2014, **150**, 55.

7 J.H.G. Bode and A.B.V. Oosterhout, *J. Lumin.*, 1975, **10**, 237.

8 G. Blasse and A.F. Corsmit, *J. Solid State Chem.*, 1973, **6**, 513.

9 C.A. Lo'pez, J. Curiale, M. del C. Viola, J.C. Pedregosa and R.D. Sa´nchez, *Physica B*, 2007, **398**, 256.

10 F. Lei and B. Yan, *J. Opt. and Adv. Mater.*, 2008, **10**, 158.

11 D.E. Bugaris, J.P. Hodges, A. Huq and H.C. Loye, *J. Solid State Chem.*, 2011, *184* 2293.

12 L. Han, L. Zhao, J. Zhang, Y. Wang, L. Guo and Y. Wang, *RSC Adv.*, 2013, **3**, 21824.

13 H. Iwakura, H. Einaga and Y. Teraoka, *J. Novel Carbon Resources Sci.*, 2011, **3**, 1.

14 M. Gateshki, J.M. Igartua and E.H. Bocanegra, *J. Phys.: Condens. Matter*, 2003, **15**, 6199.

15 X. Zhang, Z. Li, H. Zhang, S. Ouyanga and Z. Zoua, *J. Alloys Compd.*, 2009, **469**, L6.

16 V. Sivakumar and U.V. Varadaraju, *J. Solid State Chem.*, 2008, **181**, 3344.

17 P.S. Halasyamani and K.R. Poeppelmeier, *Chem. Mater.*, 1998, **10**, 2753.

18 S.L. Liu and Q. Su, Chin. *J. Chem.*, 2004, **22**, 437.

19 F. Hong, L. Zhou, L. Li, Q. Xia and X. Luo, *Optics Comm.*, 2014, **316**, 206.

20 W. Depmeier, *Acta Crystallogr. Sec. C*, 1984, **40**, 226**.**

21 B.D. Cullity, *Elements of X-ray Diffraction*, Addison-Wesley Publishing Company, USA, 1956.

22 M. Guzik, E. Tomaszewicz, S.M. Kaczmarek, J. Cybińska and H. Fuks, *J. Non-Crystalline Solids*, 2010, **356**, 1902.

23 Maheshwary, B.P. Singh, J. Singh and R.A. Singh, *RSC Adv.*, 2014, **4**, 32605.

24 E. Loh, *Phys. Rev.*, 1966, **147**, 332.

25 L. Zhang, H. Zhong, X. Li, L. Cheng, L. Yao, J. Sun, J. Zhanga, R. Hua and B. Chen, *Phys. B*, 2012, **407,** 68.

26 Y.C. Li, Y.H. Chang, Y.F. Lin, Y.S. Chang and Y.J. Lin, *J. Alloys Compd.*, 2007, **439**, 367.

27 K.V. Dabre, K. Park, S.J. Dhoble, *J. Alloys Compd.,* 2014, **617**, 129.

28 Q. Xiao, Q. Zhou and M. Li, *J. Lumin.*, 2010, **130**, 1092.

29 H. Qian, J. Zhang and L. Yin, *RSC Adv.*, 2013, **3**, 9029.

30 B.R. Judd, *Phys. Rev.*, 1962, **127**, 750.

31 G.S. Ofelt, *J. Chem. Phys.*, 1962, **37**, 511.

32 W.F. Krupke, *Phys. Rev.*, 1966, **143**, 325.

33 W.T. Carnall, H. Crosswhite, H.M. Crosswhite, Energy level structure and transition probabilities in the spectra of the trivalent lanthanides in lanthanum fluoride, *Argonne National Laboratory Report*, 1978.

34 C.K. Jorgensen, R. Reisfeld, *J. Less-Common Met.*, 1983, **93**, 107.

35 M.P. Hehlen, M.G. Brik, K.W. Krame, *J Lumin.*, 2013, **136**, 221.

36 D. Kasprowicz, M.G. Brik, A. Majchrowski, E. Michalski, E.Mykowska, *J Lumin.*, 2010, **130**, 623.

Figure Captions

Fig. 1. The schematics of citrate complexation and citrate combustion synthesis methods for the synthesis of $Ca_{4-2x}Al_6WO_{16}:RE_x,Na_x$ (RE = Eu^{3+}, Dy^{3+} and Sm^{3+}) phosphors.

Fig. 2. XRD patterns of $Ca_4Al_6WO_{16}$ synthesized by (a) citrate complexation, (b) citrate combustion methods and (c) standard JCPDS PDF #75-0697.

Fig. 3. SEM micrographs of $Ca_4Al_6WO_{16}$ synthesized by (a) citrate complexation and (b) citrate combustion methods.

Fig. 4. PL excitation spectra of $Ca_{4-2x}Al_6WO_{16}:Eu_x,Na_x$ (2mol%) phosphor with emission monitored at (a) 442nm and (b) 617nm.

Fig. 5. PL emission spectra of $Ca_{4-2x}Al_6WO_{16}:Eu_x,Na_x$ (2mol%) phosphor excited at 240nm.

Fig. 6. (a) PL emission spectra of $Ca_{4-2x}Al_6WO_{16}:Eu_x,Na_x$ (2mol%) phosphor excited at 466nm. (b) Variation of emission intensity with Eu^{3+} concentration in phosphor.

Fig. 7. PL excitation spectra of $Ca_{4-2x}Al_6WO_{16}:Dy_x,Na_x$ (2mol%) phosphor by monitoring emission at 578nm.

Fig. 8. PL emission spectra of $Ca_{4-2x}Al_6WO_{16}:Dy_x,Na_x$ (2mol%) phosphor excited at 385nm. In inset, the variation of intensity of blue (485nm) and yellow (578nm) peak with Dy^{3+} ion concentration in $Ca_4Al_6WO_{16}$ synthesized by complexation method.

Fig. 9. (a) PL excitation (λ_{em} = 604nm) spectrum of $Ca_{4-2x}Al_6WO_{16}:Sm_x,Na_x$ (2mol%) phosphor. (b) Energy level scheme of $4f^5$ configuration of Sm^{3+} ion showing various transitions related to various excitation and emission peaks.

Fig. 10. PL emission spectra of $Ca_{4-2x}Al_6WO_{16}:Sm_x,Na_x$ (2mol%) phosphor. In inset, the variation of intensity of yellow (567nm), orange-red (604nm) and red (650nm) peaks with Sm^{3+} concentration.

Fig. 11. The CIE chromaticity coordinates of $Ca_{4-2x}Al_6WO_{16}:RE_x,Na_x$ [RE = (a) Eu, (b) Dy and (c) Sm] phosphors on 1931 CIE chromaticity diagram.

Table 1. Intensity parameters $\Omega_{(k)}$ (k = 2,4,6) (in the unit of 10^{-20} cm^2) of $CaAl_6WO_{16}:RE^{3+}$ (RE = Eu, Dy and Sm) phosphors.

Table 2. Luminescence parameters for Eu^{3+}, Dy^{3+} and Sm^{3+} ions activated $CaAl_6WO_{16}$ phosphor at room temperature.

Fig. 1.

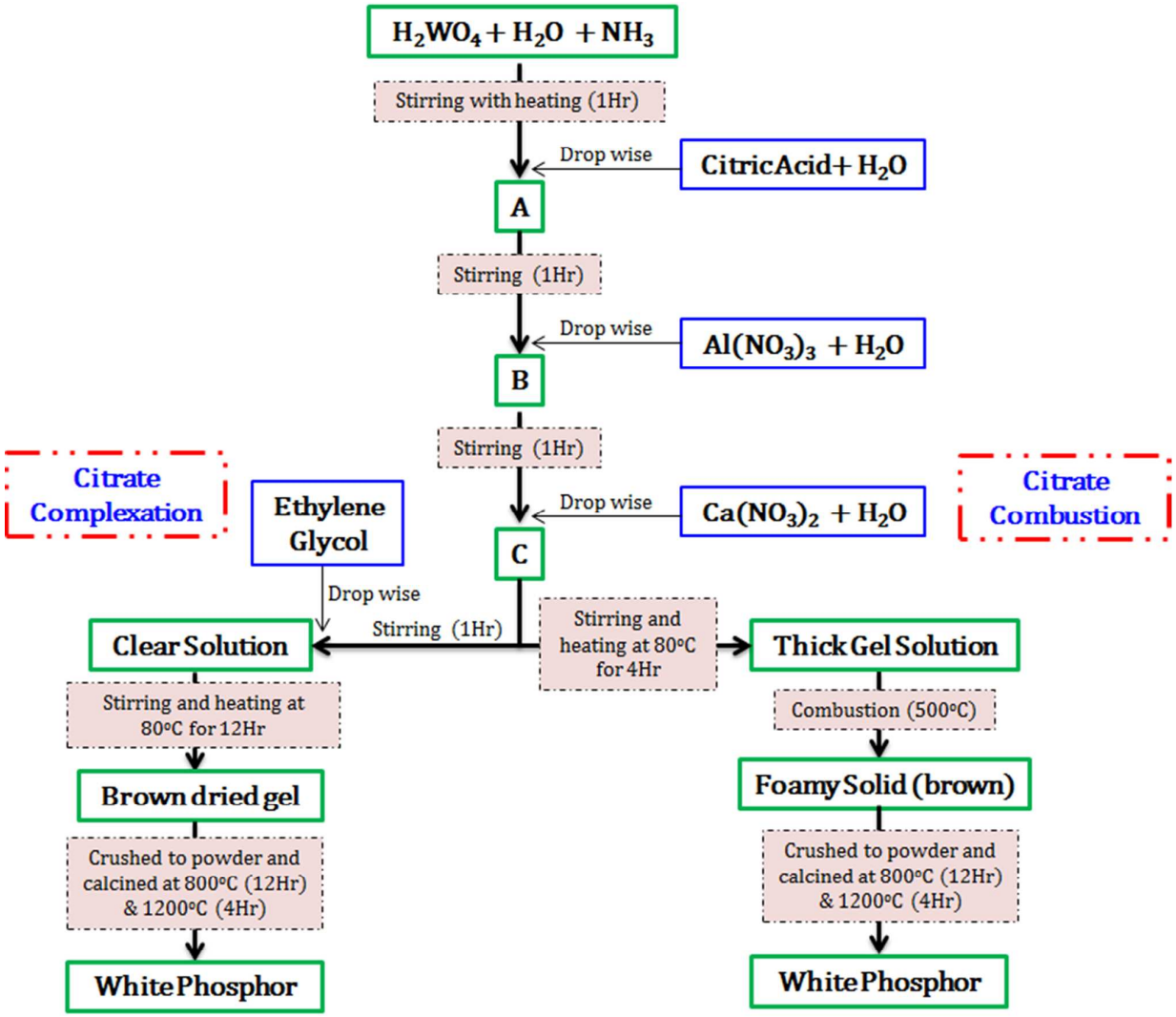
$H_2WO_4 + H_2O + NH_3$
Stirring with heating (1Hr)
Drop wise
Citric Acid + H_2O
A
Stirring (1Hr)
Drop wise
$Al(NO_3)_3 + H_2O$
B
Stirring (1Hr)
Drop wise
$Ca(NO_3)_2 + H_2O$
C
Citrate Complexation
Ethylene Glycol
Citrate Combustion
Drop wise
Stirring (1Hr)
Clear Solution
Stirring and heating at 80°C for 4Hr
Thick Gel Solution
Stirring and heating at 80°C for 12Hr
Combustion (500°C)
Brown dried gel
Foamy Solid (brown)
Crushed to powder and calcined at 800°C (12Hr) & 1200°C (4Hr)
Crushed to powder and calcined at 800°C (12Hr) & 1200°C (4Hr)
White Phosphor
White Phosphor

Fig. 2.

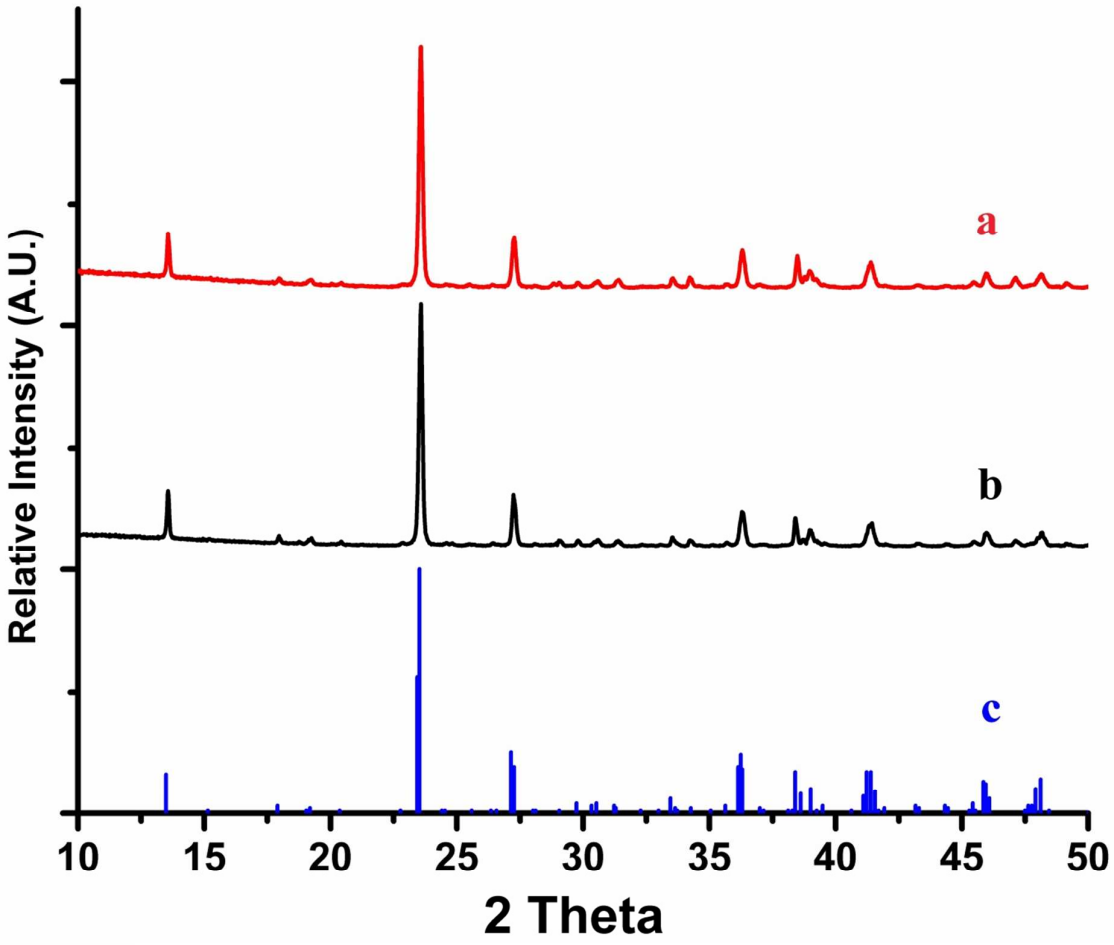

Fig. 3.

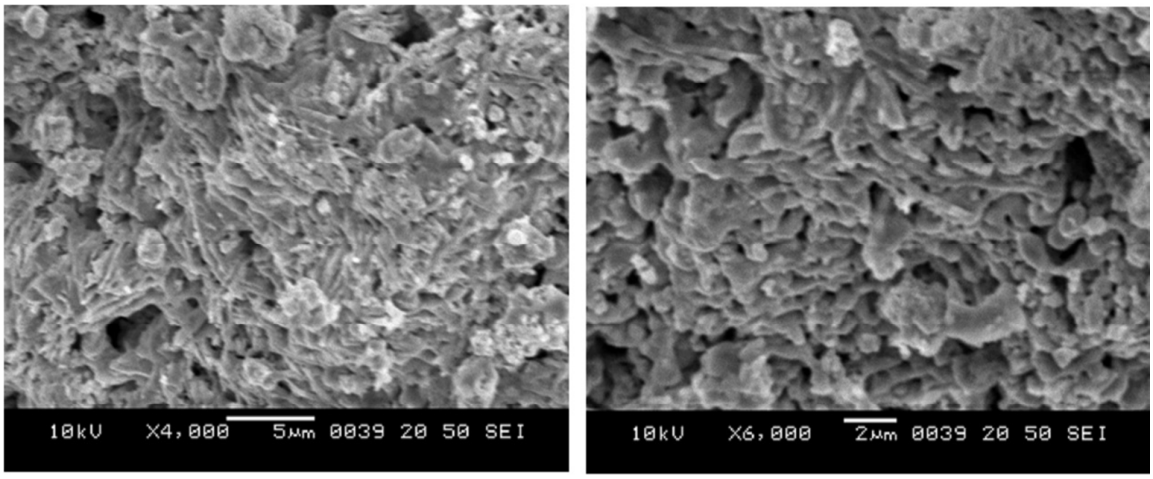
10kV X4,000 5μm 0039 20 50 SEI
10kV X6,000 2μm 0039 20 50 SEI

a

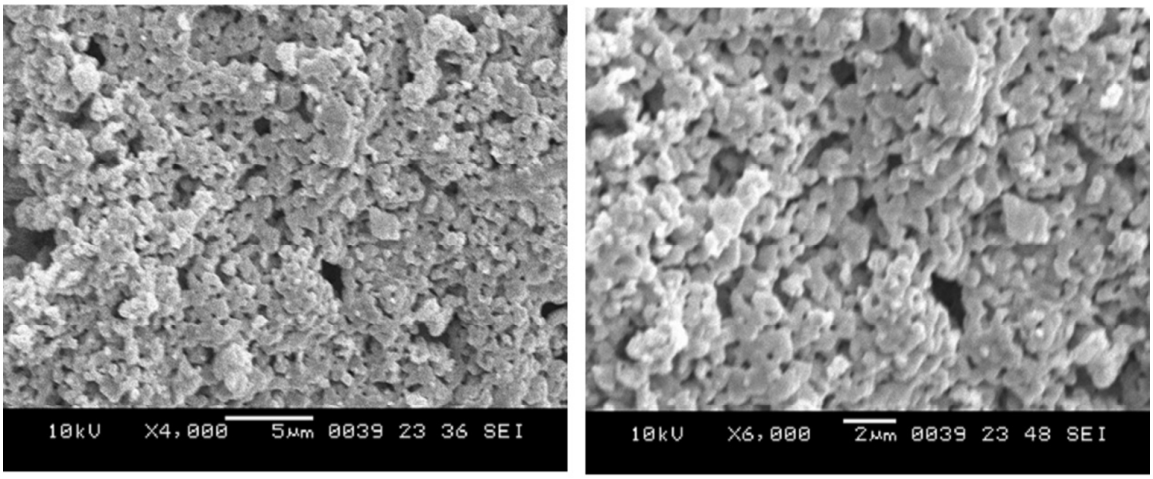
10kV X4,000 5μm 0039 23 36 SEI
10kV X6,000 2μm 0039 23 48 SEI

b

Fig. 4.

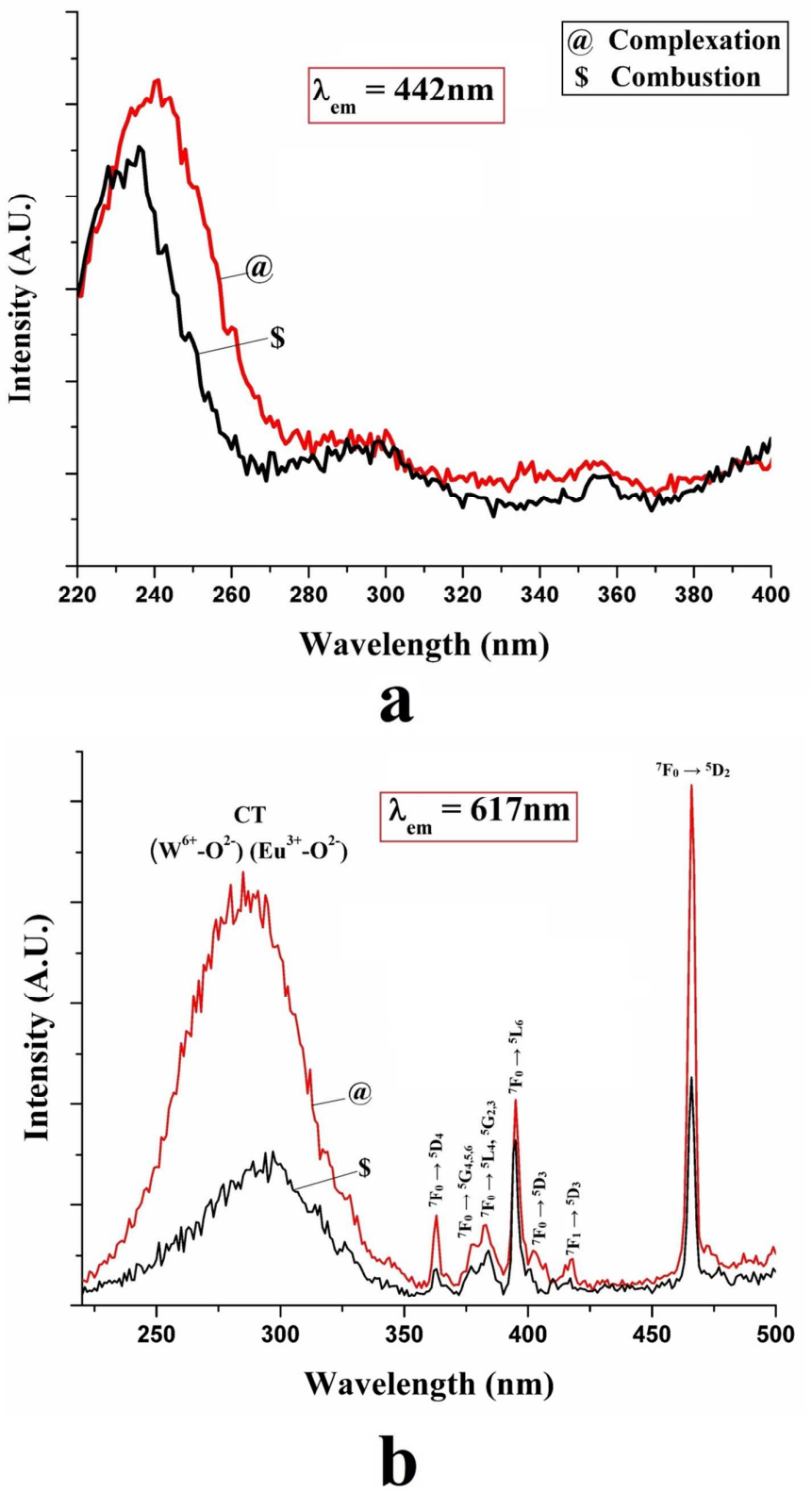
@ Complexation
$ Combustion
λem = 442nm
Intensity (A.U.)
@
$
220 240 260 280 300 320 340 360 380 400
Wavelength (nm)
a
λem = 617nm
CT
(W6+-O2-) (Eu3+-O2-)
7F0 → 5D2
7F0 → 5L6
7F0 → 5D4
7F0 → 5G4,5,6
7F0 → 5L4, 5G2,3
7F0 → 5D3
7F1 → 5D3
Intensity (A.U.)
@
$
250 300 350 400 450 500
Wavelength (nm)
b

Fig. 5.

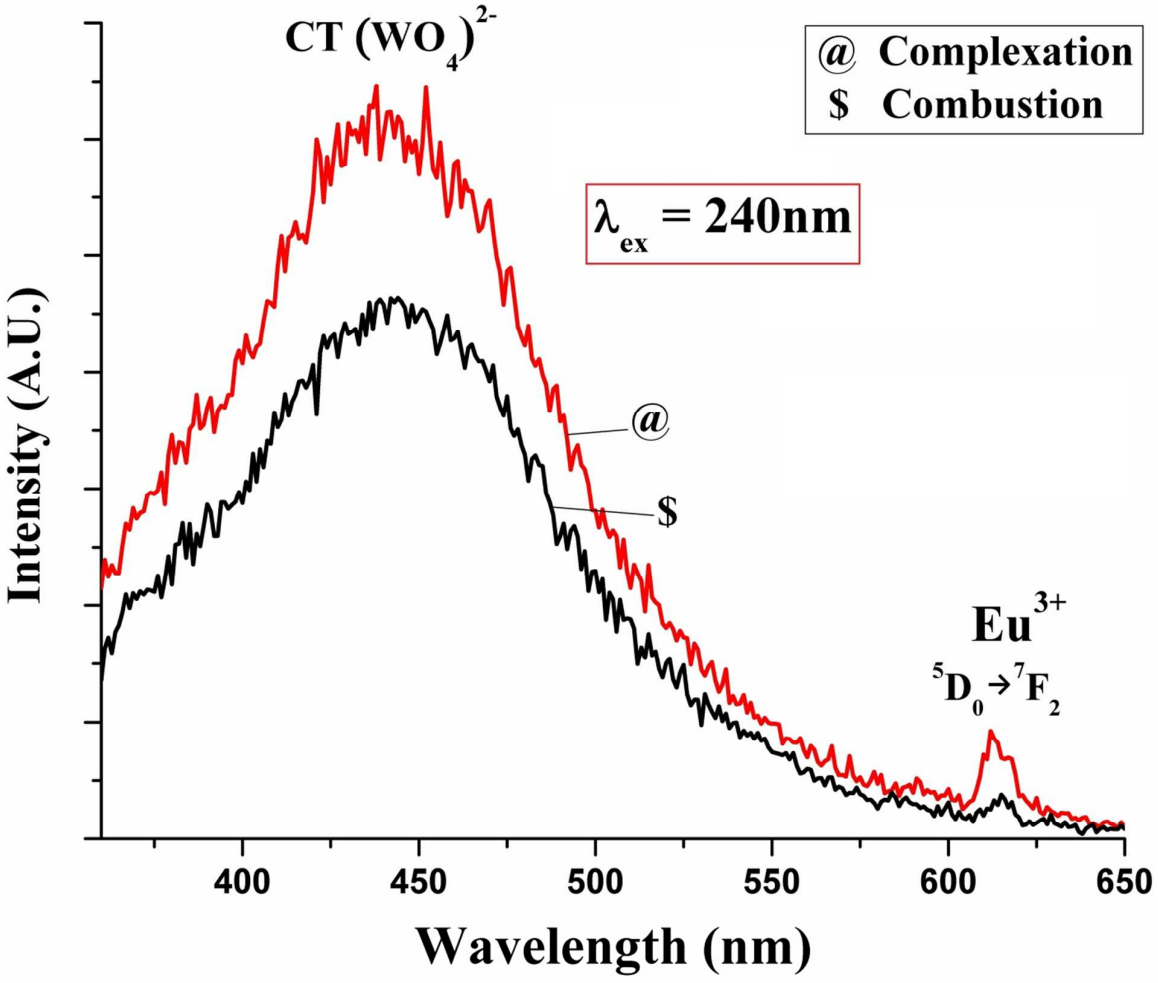
CT $(WO_4)^{2-}$
@ Complexation
$ Combustion
λ_{ex} = 240nm
@
$
Eu^{3+}
$^5D_0 \rightarrow {}^7F_2$
Intensity (A.U.)
400
450
500
550
600
650
Wavelength (nm)

Fig. 6.

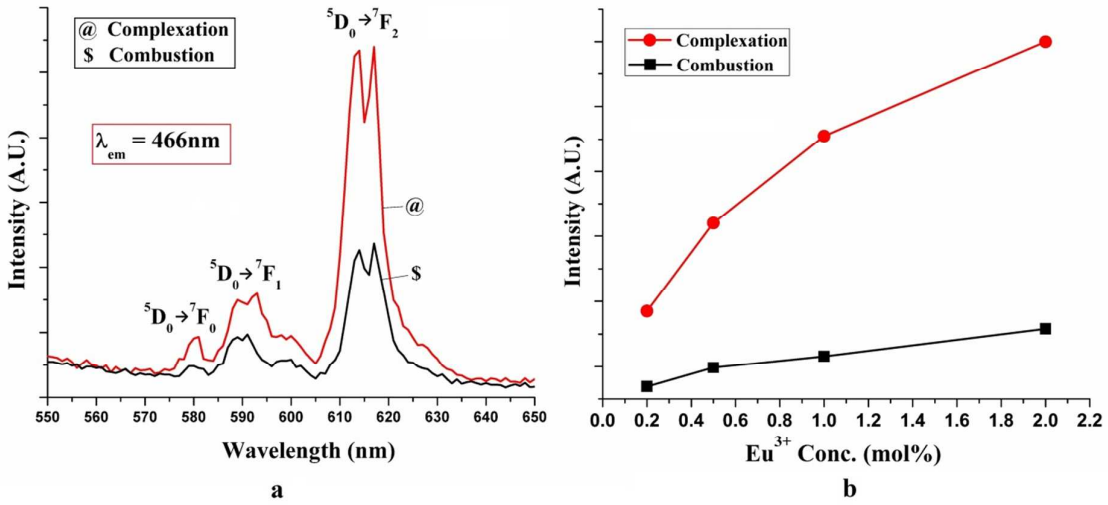
@ Complexation
$ Combustion
λem = 466nm
5D0→7F2
5D0→7F1
5D0→7F0
@
$
Intensity (A.U.)
Wavelength (nm)
a
Complexation
Combustion
Intensity (A.U.)
Eu3+ Conc. (mol%)
b

Fig. 7.

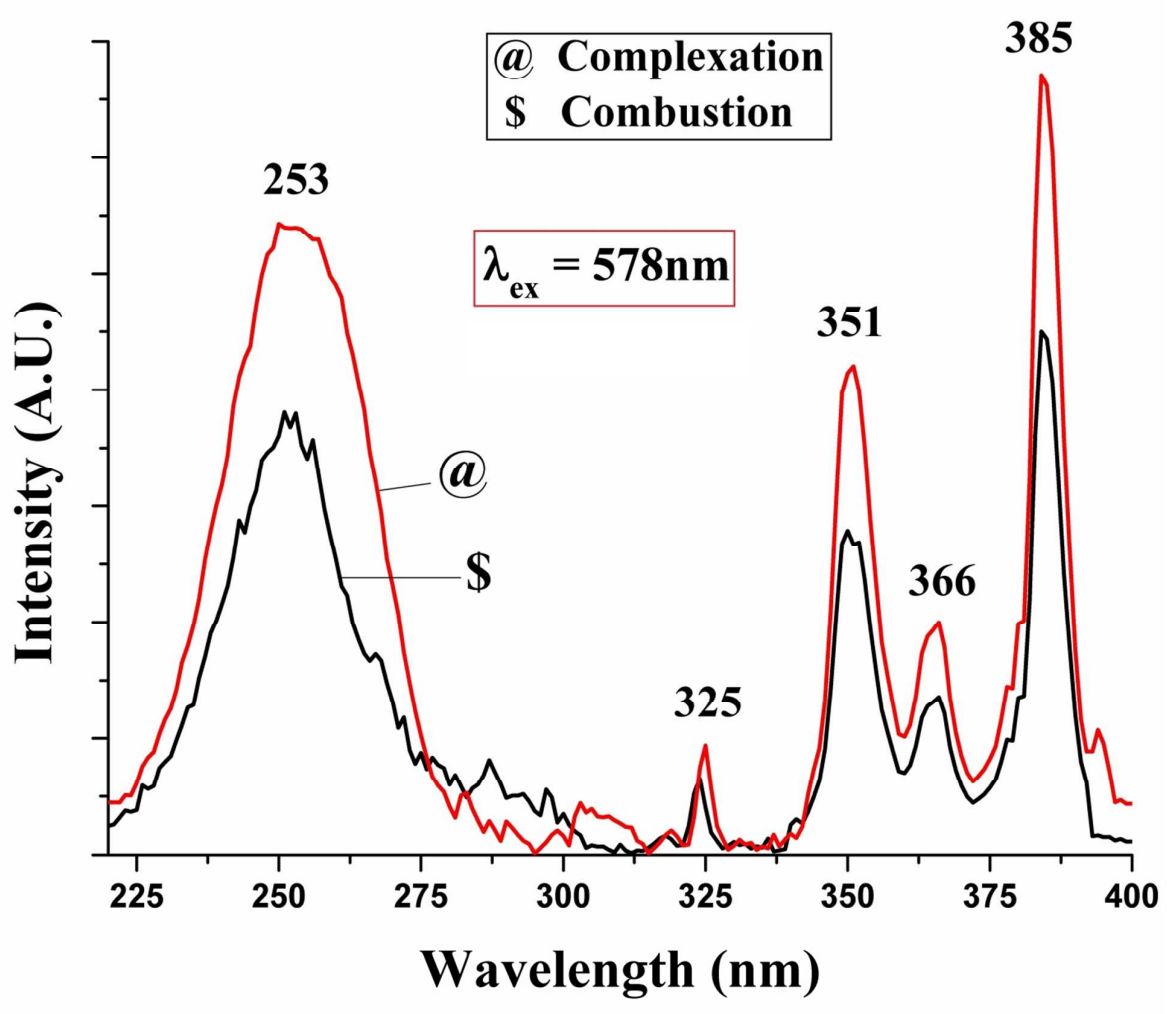
@ Complexation
$ Combustion
λex = 578nm
253
325
351
366
385
@
$
Intensity (A.U.)
225
250
275
300
325
350
375
400
Wavelength (nm)

Fig. 8.

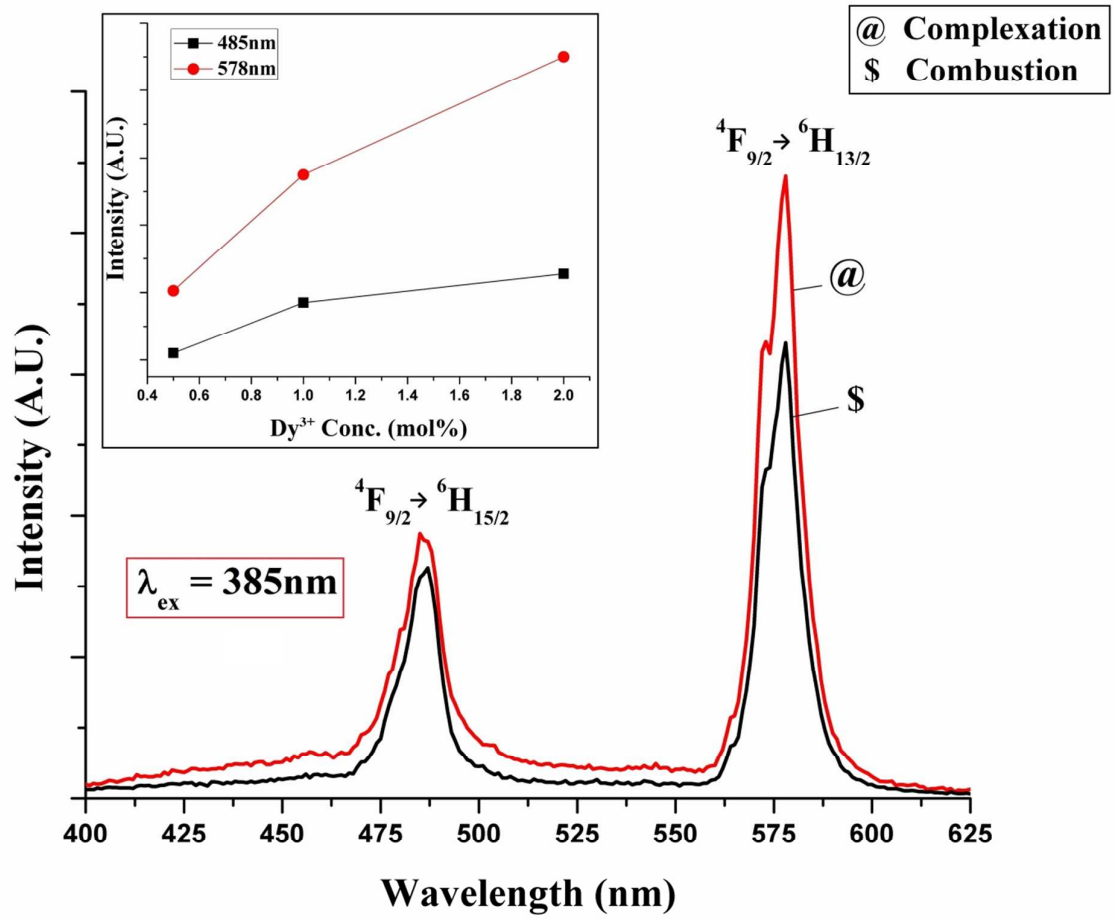
@ Complexation
$ Combustion
485nm
578nm
Intensity (A.U.)
Dy3+ Conc. (mol%)
0.4 0.6 0.8 1.0 1.2 1.4 1.6 1.8 2.0
4F9/2→ 6H13/2
@
$
4F9/2→ 6H15/2
λex = 385nm
Intensity (A.U.)
400 425 450 475 500 525 550 575 600 625
Wavelength (nm)

Fig. 9.

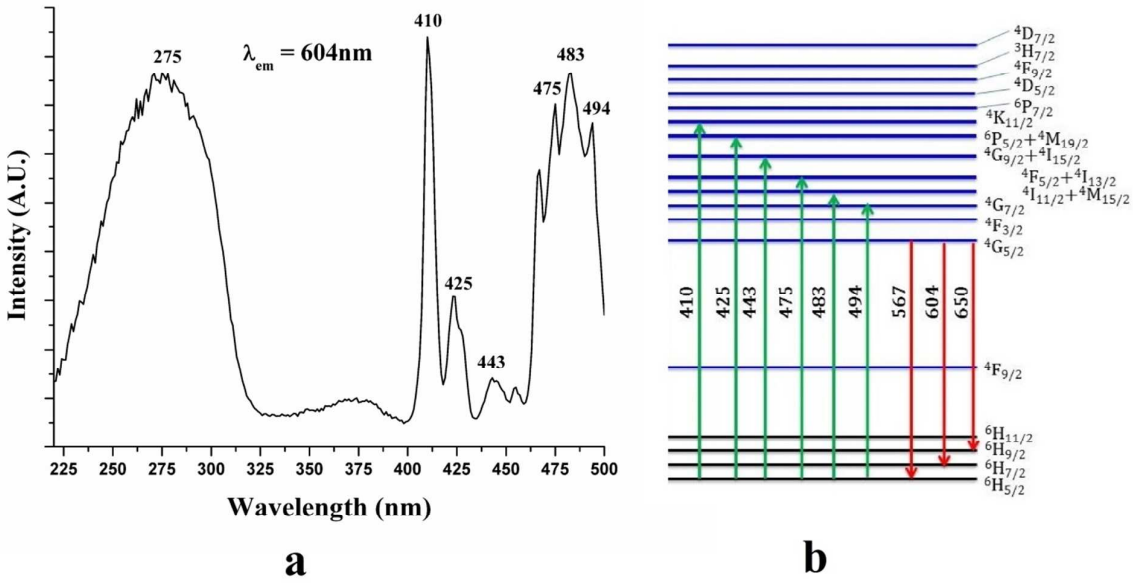
275
λem = 604nm
410
483
475
494
425
443
Intensity (A.U.)
225 250 275 300 325 350 375 400 425 450 475 500
Wavelength (nm)
a
4D7/2
3H7/2
4F9/2
4D5/2
6P7/2
4K11/2
6P5/2+4M19/2
4G9/2+4I15/2
4F5/2+4I13/2
4I11/2+4M15/2
4G7/2
4F3/2
4G5/2
410
425
443
475
483
494
567
604
650
4F9/2
6H11/2
6H9/2
6H7/2
6H5/2
b

Fig. 10.

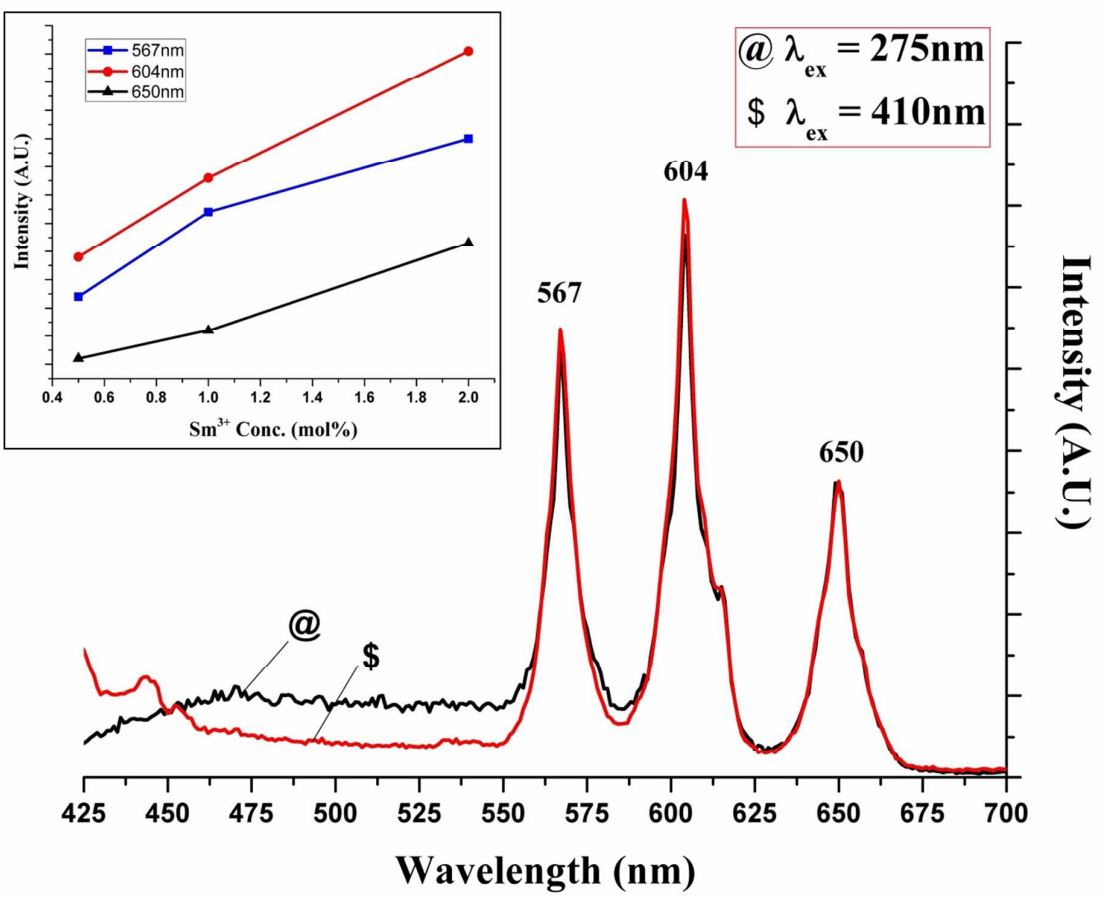
567nm
604nm
650nm
Intensity (A.U.)
0.4 0.6 0.8 1.0 1.2 1.4 1.6 1.8 2.0
Sm3+ Conc. (mol%)
@ λex = 275nm
$ λex = 410nm
567
604
650
@
$
Intensity (A.U.)
425 450 475 500 525 550 575 600 625 650 675 700
Wavelength (nm)

Fig. 11.

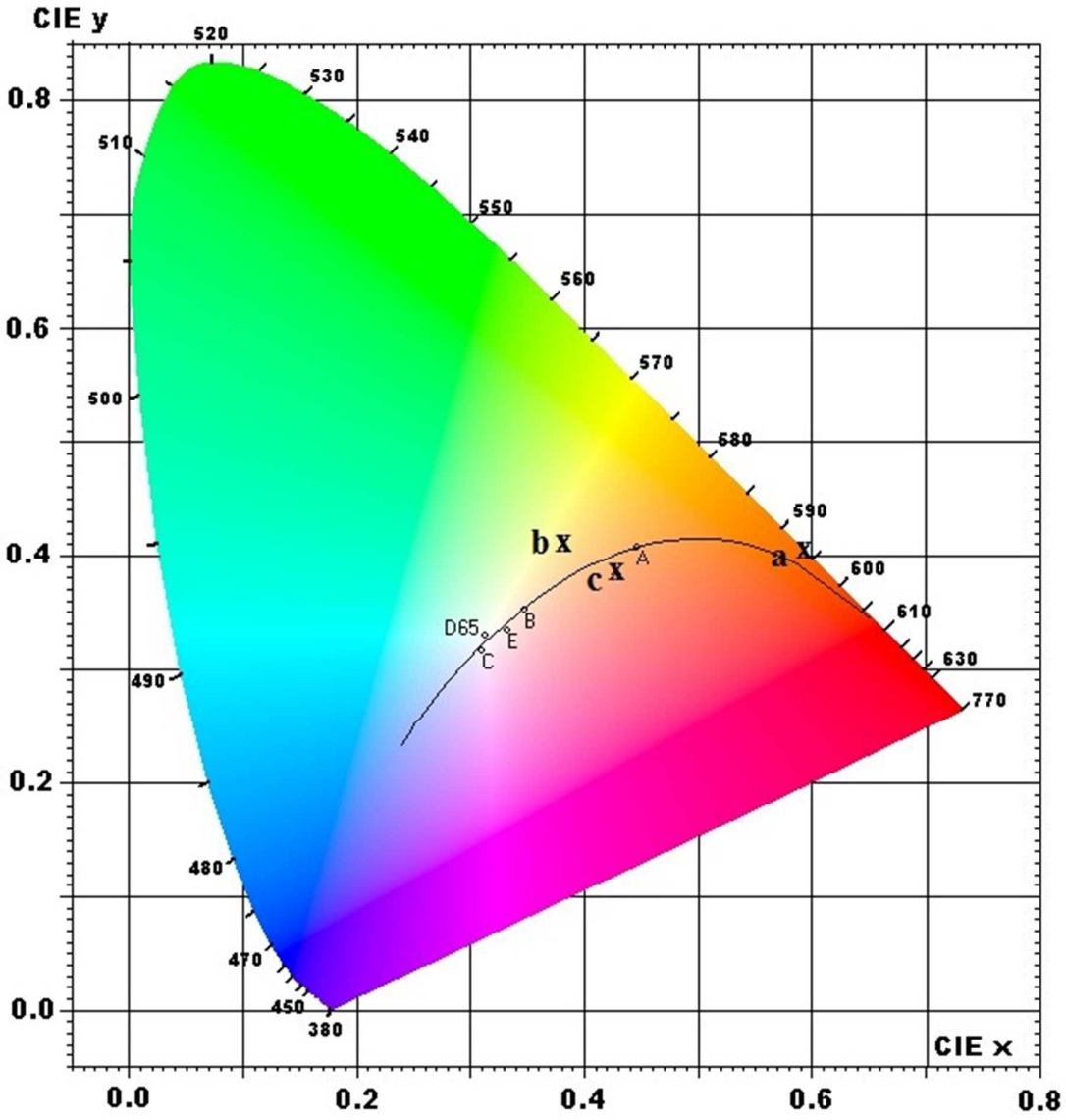
CIE y
CIE x
0.0
0.2
0.4
0.6
0.8
520
530
540
550
560
570
580
590
600
610
630
770
510
500
490
480
470
450
380
b x
c x
a x
A
B
C
D65
E

Table 1.

	$\Omega_{(2)}$	$\Omega_{(4)}$	$\Omega_{(6)}$
$CaAl_6WO_{16}:Eu^{3+}$	4.69	---	---
$CaAl_6WO_{16}:Dy^{3+}$	3.92	2.85	---
$CaAl_6WO_{16}:Sm^{3+}$	5.26	2.18	0.94

Table 2.

RE^{3+}	Transition	$A_{J\rightarrow J'}$	β	τ_{rad} (ms)
Eu^{3+}	$^5D_0\rightarrow{}^7F_1$	262	0.38	
	$^5D_0\rightarrow{}^7F_2$	422	0.62	
		$\sum A_{J\rightarrow J'} = 684$		1.46
Dy^{3+}	$^4F_{9/2}\rightarrow{}^4H_{15/2}$	174	0.28	
	$^4F_{9/2}\rightarrow{}^4H_{13/2}$	454	0.72	
		$\sum A_{J\rightarrow J'} = 628$		1.59
Sm^{3+}	$^4G_{5/2}\rightarrow{}^6H_{5/2}$	216	0.27	
	$^4G_{5/2}\rightarrow{}^6H_{7/2}$	384	0.48	
	$^4G_{5/2}\rightarrow{}^6H_{9/2}$	196	0.25	
		$\sum A_{J\rightarrow J'} = 796$		1.26